Hindawi
Advances in Civil Engineering
Volume 2019, Article ID 9256260, 12 pages
https://doi.org/10.1155/2019/9256260

Research Article

Estimation of Elastic Properties of Oil Palm Kernel Shell Concrete by Semianalytical Methods of Homogenisation

Mohamed Gibigaye,[1] **Fructueux Gildas Godonou**,[1] **Crespin Prudence Yabi**,[2] **and Gerard Degan**[2]

[1]*Civil Engineering Department, Polytechnic School of Abomey-Calavi, University of Abomey-Calavi, Cotonou 01 BP 2009, Benin*
[2]*National University of Sciences, Technologies, Engineering and Mathematics of Abomey, Abomey, Benin*

Correspondence should be addressed to Mohamed Gibigaye; mohamed.gibigaye@uac.bj

Received 11 June 2019; Revised 5 August 2019; Accepted 16 August 2019; Published 8 September 2019

Academic Editor: Evangelos J. Sapountzakis

Despite its importance as one of the key parameters in the design of structural elements, the modulus of elasticity (MoE) is one of the least researched areas in oil palm kernel shell (OPKS) concrete. In the present study, we determined the MoE of OPKS concrete, using micromechanical models based on the classic approaches of homogenisation of Hashin–Shtrikman (HS) and Mori–Tanaka (MT). The MoE values for OPKSC ($f_{cu} < 35$ MPa and OPKS volume fraction < 42%) estimated using the HS and MT models in the literature showed a good correlation with the experimental values. An empirical linear correlation between the volume fraction of inclusions and the MoE was proposed. The results obtained can enable better control of the mix design of structural concrete based on the proportion of OPKS coarse aggregate in tropical countries producing palm oil.

1. Introduction

For the efficient use of concrete in the design of structural elements in civil engineering, professionals need to be aware of the elastic properties of the concrete, particularly its modulus of elasticity (MoE) or Young's modulus or *E*-value. The MoE of structural concrete is a mechanical property that reflects its ability to deform elastically under loading. Because concrete is widely used in the elastic range of deformations in the structural design of elements, the knowledge of the MoE of concrete aids in avoiding excessive deformation of the structural elements, providing satisfactory serviceability and achieving the most cost-effective design [1]. Several authors have established that concrete made from oil palm kernel shell (OPKS) can be used as structural concrete in the elements of small- and medium-scale buildings [2–8]. According to Alengaram et al. [9], despite its importance as one of the key parameters in the design of structural elements, the MoE is one of the least researched areas in OPKS concrete.

Until recently, few references were available in the literature concerning the MoE of OPKS concrete [6,10–18], out of which few were concerned with its theoretical determination. In his theoretical approach for the determination of the MoE of OPKS concrete, Alengaram et al. [6] used a modified form of the empirical equation of prediction, proposed by the code, CEB/FIP (MC2010). Ahmmad et al. [13] explained that the prediction equation reported by Alengaram underestimated the MoE of OPKSC and derived a new equation by comparing the MoE with the compressive strength. Aslam et al. [16] compared the MoE values of OPKS estimated using Alengaram's equation with those estimated using other equations proposed in the literature to predict the MoE of LWACs and concluded that Alengaram's equation provides results that are closest to the experimental results. According to Mannan and Ganapathy [12], the MoE of OPKSC is strongly influenced by the intrinsic properties (such as stiffness) of the composite's two constitutive phases, i.e., the cement paste and the OPKS. The equations proposed by Alengaram et al. and Ahmmad et al.

indicate that the MoE of OPKSC depends on its compressive strength and density. Thus, these equations did not directly consider the stiffness of the inclusions (OPKS).

In the process of determination of the MoE of OPKS concrete, the technique of homogenisation of the composite simultaneously considered the intrinsic properties of the two constitutive phases. Homogenisation is a modelling technique that assimilates a heterogeneous material to a fictitious homogeneous equivalent material for which we need to determine the characteristics. The homogeneous equivalent material must exhibit the same overall mechanical behaviour, meet the same boundary conditions, and respect the principle of conservation of energy [19]. This approach of homogenisation has been successfully applied to other composite materials, such as expanded clays, and resin mortar [19, 20].

In this study, we determined the MoE of OPKS concrete, using micromechanical models based on the classic approaches of homogenisation of Hashin–Shtrikman (HS) and Mori–Tanaka (MT), and validated the results obtained through a comparison with those obtained experimentally from the works of previous authors.

The paper is organised into three sections. First, the physical and mechanical properties of the OPKS components are described. The experimental mix proportions used in the micromechanical study on the composite are also detailed in this section.

The second section of this article focuses on the homogenisation technique used in this study based on the Eshelby problem for the estimation of elastic properties of the isotropic two-phase OPKSC composite. Here, we also validate the proposed method by comparing the predicted values of the MoE for a similar composite presented in the literature (epoxy resin) with the results for this composite.

In the final section, the MoE values for OPKSC predicted using different numerical micromechanical models are presented and compared with the experimental results given in the literature.

2. Materials and Methods

2.1. Experimental Program

2.1.1. Materials and Mix Proportions. For this study, we used an OPKS concrete grade-20. The constituents used in the mix were those indicated in the study [21]. The properties of the constituents used are presented in Table 1.

For an aggregate size of 2–8 mm, the flakiness index for OPKS is greater than 70%, as can be seen in Table 1. This means that they exhibit an elongated shape and therefore can be modelled by ellipsoids.

We used the mix proportion of cement : sand : OPKS in weights of 1 : 1.53 : 0.99 with a cement content of 450 kg/m^3 and water per cement equal to 0.45 [21].

2.1.2. Specimen Preparation. We prepared three cylinders in steel moulds, each with a diameter of 11 cm and a height of 22 cm, in accordance with NF EN 12390-1. Next, in accordance with NF EN 12390-2, after casting, we placed the specimens in the laboratory at ambient conditions (24–28°C; relative humidity: 80–93%) for 24 h before they were demoulded. After demoulding, we placed the specimens in water at 20 ± 2°C until the moment of micromechanical study on OPKS concrete.

Table 1: Physical properties of constituents of OPKS concrete grade-20 [21].

Properties	Constituents	
	Sand	OPKS
Specific gravity	2.59	1.31
Loose bulk density (kg/m^3)	1410	530
Water absorption, 24 h (%)	—	19.93
Fineness modulus	2.4	—
Aggregate abrasion value (Los Angeles) (%)	—	5.02
Size (mm)	0–5	2–8
Flakiness index	—	70.27%
Type of cement	CEM II 32.5	

2.2. Semianalytical Determination of MoE Using Homogenisation Techniques. Homogenisation is a modelling technique that assimilates a heterogeneous material to a fictitious homogeneous equivalent material, as depicted in Figure 1 [22]. It incorporates three essential steps [23]: (i) representation, (ii) localisation, and (iii) homogenisation.

Similar [20] to the case of eco-friendly composite materials, we considered the OPKSC to consist of two phases: the cement matrix and inclusions (OPKS).

2.2.1. Step 1: Representation. Here, two tasks need to be achieved: (i) to experimentally determine the mechanical properties (Young's modulus and Poisson's ratio) of each of the two phases of the composite and (ii) to choose a representative minimum volume of the composite, known as representative volume element (RVE). For simplification purposes, using the physical properties in Table 1, the mechanical properties of each of the two phases of the composite in this study were obtained from the works of previous authors (Table 2).

The size of the RVE, which had a cubic form, was determined based on the work of Wiacek et al. [28], who concluded that the dimensions have to satisfy the condition, $l \geq 5 \times d_{\max}$, where l is the dimension of the side of the RVE and $d_{\max}$ is the maximum diameter of the OPKS. According to Table 1, $d_{\max} = 8$ mm. Therefore, $l \geq 5d_{\max} \Longrightarrow l \geq 40\ \text{mm} = l_{\min}$.

To study the fluctuations in the macroscopic properties of the composite, four sizes of the cubic RVE, which characterises the microstructure of the composite, were considered: 40, 50, 60, and 70 mm. Figure 2 illustrates how the different sizes of RVE were obtained.

2.2.2. Step 2: Localisation. The localisation is concerned with the determination of the local properties of the RVE, namely, the stiffness of each of the two phases of the composite, shape ratio, volume fraction, and geometric orientation of inclusions in the cement matrix.

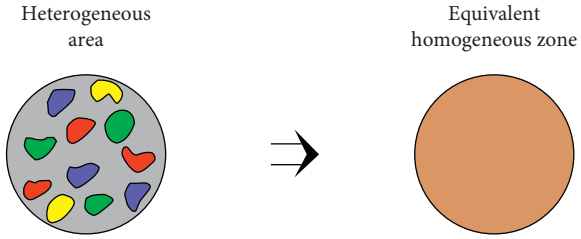

Figure 1: Principle of homogenisation of a composite: hypothesis of the same macroscopic behaviour [22].

Table 2: Young's modulus and Poisson's ratio of OPKS and cement matrix.

Phases	Young's modulus, E (GPa)	Poisson's ratio ν
OPKS	2.25 [24]	0.19 [25]
Cement matrix	10.00 [26, 27]	0.19 [26, 27]

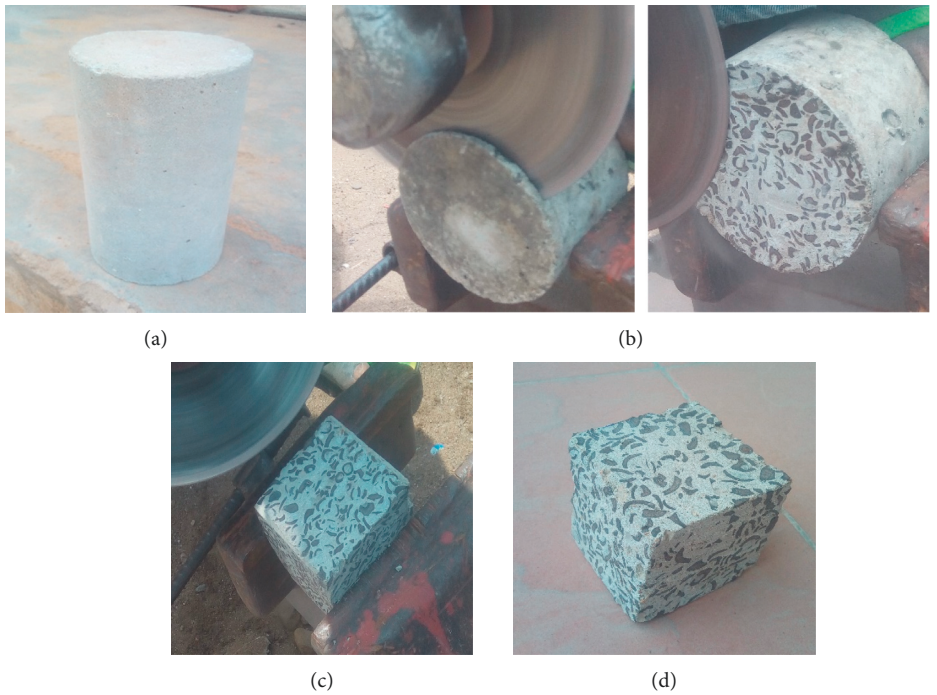

Figure 2: Process of obtaining RVE: (a) whole sample, (b) cutting of the test specimen, (c) grinding and smoothing of faces, and (d) cubic sample.

Assuming that the two phases of the composite are elastic and isotropic at the microscopic level, the general form of the tensor of stiffness of the cement matrix and inclusions can be defined as follows [29]:

$$C = \begin{bmatrix} \lambda + 2\mu & \lambda & \lambda & 0 & 0 & 0 \\ \lambda & \lambda + 2\mu & \lambda & 0 & 0 & 0 \\ \lambda & \lambda & \lambda + 2\mu & 0 & 0 & 0 \\ 0 & 0 & 0 & \mu & 0 & 0 \\ 0 & 0 & 0 & 0 & \mu & 0 \\ 0 & 0 & 0 & 0 & 0 & \mu \end{bmatrix}, \quad (1)$$

where λ and μ are Lame's coefficients for each of the two phases of the composite, with

$$\lambda = \frac{E\nu}{(1+\nu)(1-2\nu)}, \qquad \mu = \frac{E}{2(1+\nu)}. \quad (2)$$

For all four sizes of the RVE, we used a classic scanner (the one used for scanning printed documents) for the acquisition of digital images of the six faces of the cubic sample, as illustrated in Figure 3. Using ImageJ software

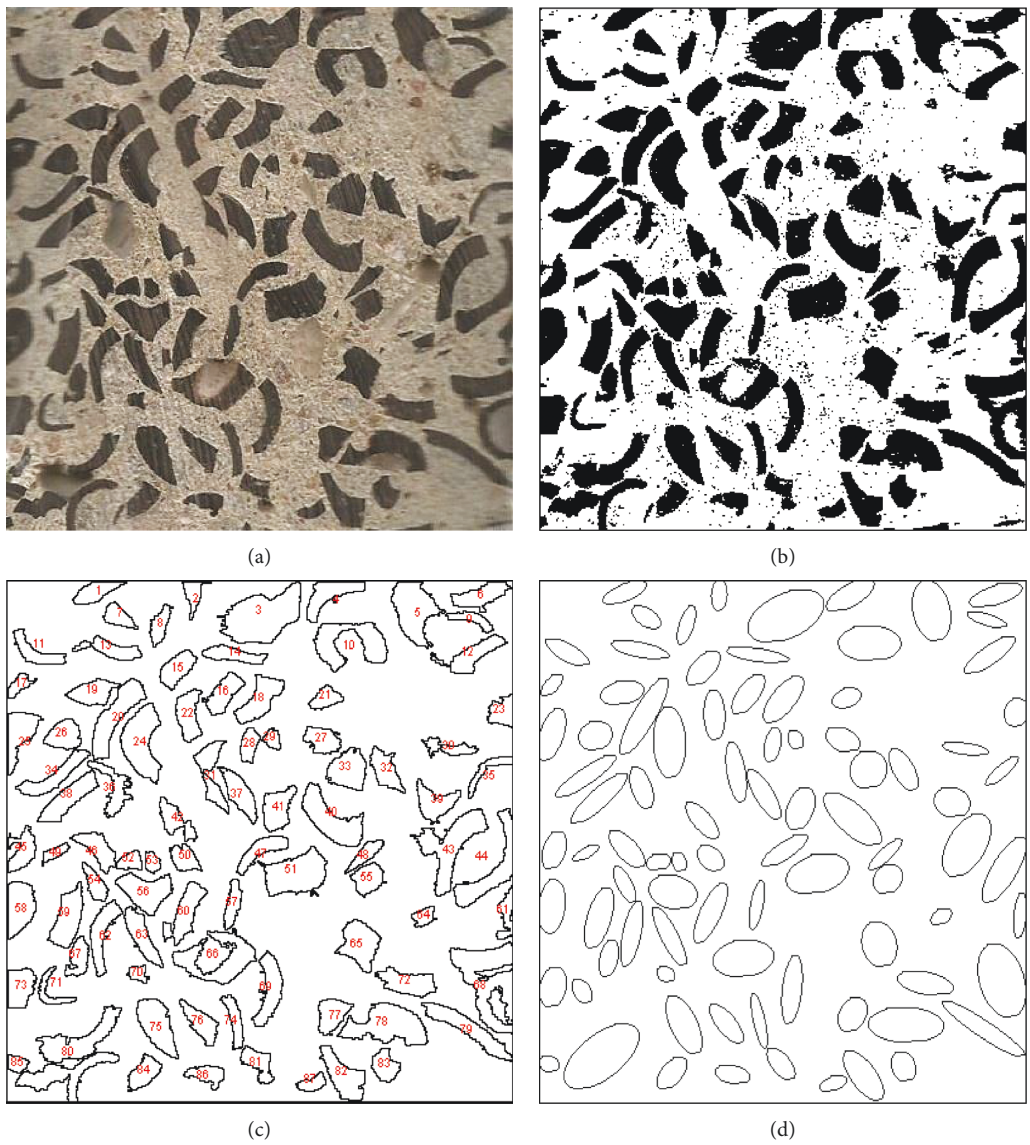

Figure 3: Procedure for image processing of RVE faces for OPKSC. (a) Original scanned image. (b) Binarised image obtained after thresholding, using by ImageJ®. (c) Image depicting the labelled particles. (d) Image depicting the adjustment of ellipses on the particles (geometric modelling).

(URL: http://rsb.info.nih.gov/ij/download.html), digital images of each of the faces of the RVE were processed to obtain binary images, through thresholding, as illustrated in Figure 3. In the binarised image, the particles of OPKS are depicted by the black pixels and the cement matrix is depicted by the white pixels.

For each particle detected in the binarised image (Figure 3(c)), the area and perimeter were generated and stored in the software. The length and width of the detected particles (maximum diameter and minimum diameter of Feret [30, 31]) were defined from the ellipse that models the particle, as illustrated in Figure 4.

For each side of each of the four sizes of the RVE, the identification results are presented in Table 3.

In Table 3, A_i represents the area of the particle i, X_i and Y_i are the coordinates of the barycentre, L_i and D_i are the lengths corresponding to the major and the minor axes of the ellipse, and φ_i is the orientation angle of the major axis of the ellipse with respect to an axis of reference (Figure 5) [19]. The direction of the axis of the ellipse is the centre line of the smaller rectangle containing the particle.

From the data in Table 3, the components of orientation tensor, average shape ratio r, and volume fraction v_c of OPKS were determined by equations (3) and (5):

$$a_{ij} = \frac{1}{N} \sum_{k=1}^{N} p_i^k p_j^k, \tag{3}$$

where N is the number of particles, p_i and p_j are the components of the unit vector p, determined by equation (4) with $\theta = \pi/2$ for a 2D analysis:

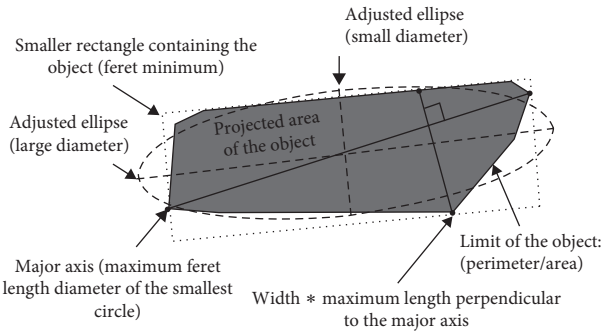

Figure 4: Analysed widths and lengths [30].

Table 3: General presentation of data from image analysis.

Particle	Area (A_i)	X_M	Y_M	Major (L)	Minor (D)	Angle φ (°C)
1	A_1	X_1	Y_1	L_1	D_1	φ_1
...	...	...	...	...	...	...
i	A_i	X_i	Y_i	L_i	D_i	φ_i
...	...	...	...	...	...	...
N	A_N	X_N	Y_N	L_N	D_N	φ_N

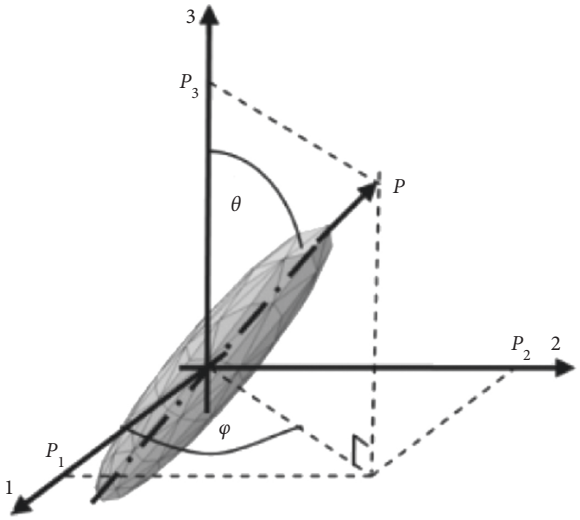

Figure 5: Particle orientation [19].

$$p_1 = \sin\theta\cos\varphi,$$
$$p_2 = \sin\theta\sin\varphi, \quad (4)$$
$$p_3 = \cos\theta.$$

The set of the a_{ij} of the RVE defines a tensor of order 2, rated a_2:

$$r = \frac{\sum_{i=1}^{N} A_i \cdot (L_i/D_i)}{\sum_{i=1}^{N} A_i},$$
$$V_c = \frac{\sum_{i=1}^{N} A_i}{A_{\text{face}}}. \quad (5)$$

Figure 6 illustrates the scanned images of the six faces obtained for one of the four sizes of the RVE, i.e., $60 \times 60 \times 60\,\text{mm}^3$.

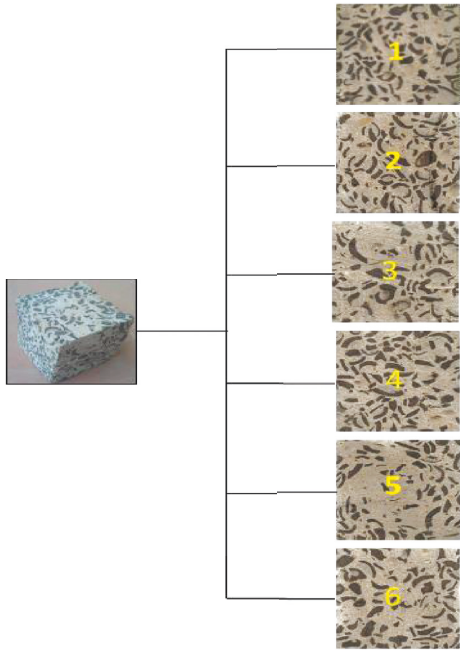

Figure 6: Scanned images of the six faces of the RVE of size $60 \times 60 \times 60\,\text{mm}^3$.

Information on the distribution of the size and orientation of the particles on side 1 of the RVE of $60 \times 60 \times 60\,\text{mm}^3$ is summarised (in extract) in Table 4.

Table 5 summarises the values of the volume fraction, average shape ratio, and components of the tensor a_2, obtained for a random distribution in 2D on each of the faces of the RVE of $60 \times 60 \times 60\,\text{mm}^3$.

Several types of orientation can be considered for the particles inside the RVE. In the case of the present composite, Figure 7 illustrates some geometric examples of orientation with the corresponding tensors [32].

In the orientation tensor a_2 of Table 5, the values of the components a_{11} and a_{22}, and a_{12} and a_{21} were close to 0.5 and 0, respectively, as in the case of the components of the tensor a_2 for the 2D random orientation (see Figure 7(b)). The relative difference between the two cases was of the order of 5%. This confirms that the traces of the particles appearing on different sides of the cubic RVE were not arranged in a particular orientation. Thus, we conclude that there exists a 2D random distribution on each of the faces of the RVE. At the 3D scale, by extension, we retain a random distribution. Based on Figure 7(a), we concluded that, at the scale of the RVE, the composite is considered as an isotropic medium in view of the random orientation of the particles.

The volume fractions and shape ratios of OPKS varied minimally from one face to another with a standard deviation of the volume fraction of 2.7% and a shape ratio of 0.22. In the remainder of the homogenisation procedure, for simplification purposes, we will use the average values of the volume fractions and shape ratios of the OPKS obtained on the faces of the RVE.

Table 6 summarises the mean values of the volume fraction and shape ratio for all four sizes of the RVE considered in this study.

Table 4: Extract of data from image analysis of side 1 of the RVE of $60 \times 60 \times 60\,\text{mm}^3$ (see Section 1 in Supplementary Material).

Particle	Area (A_i)	X_M	Y_M	Major (L)	Minor (D)	Angle ϕ (°C)
1	8.842	10.433	1.115	5.724	1.967	20.851
2	5.603	22.048	1.431	3.628	1.966	87.138
3	41.265	30.256	3.983	10.073	5.216	22.752
4	13.477	38.205	1.537	6.602	2.599	28.297
5	25.965	48.304	3.301	7.176	4.607	104.35
6	12.24	56.309	1.531	6.749	2.309	16.210
7	6.547	13.107	3.979	3.946	2.112	149.53
.	.	.	.	.	.	.
.	.	.	.	.	.	.
.	.	.	.	.	.	.
87	4.432	36.193	57.752	3.536	1.596	18.128

Table 5: Fraction volumes, average shape ratio, and components of the tensor a_2 on each of the faces of the RVE of $60 \times 60 \times 60\,\text{mm}^3$.

	Components of the tensor a_2			r	v_c (%)
	a_{11}	a_{22}	$a_{12} = a_{21}$		
Face 1	0.496	0.504	0.043	2.381	31.7
Face 2	0.419	0.581	−0.068	2.714	30.0
Face 3	0.491	0.509	−0.021	2.476	26.5
Face 4	0.665	0.335	−0.040	2.676	32.6
Face 5	0.524	0.476	−0.0085	3.007	24.5
Face 6	0.556	0.444	0.035	2.294	31.1
Average	0.525	0.475	−0.009	2.591	29.4
Standard deviation	0.069	0.069	0.036	0.221	2.704

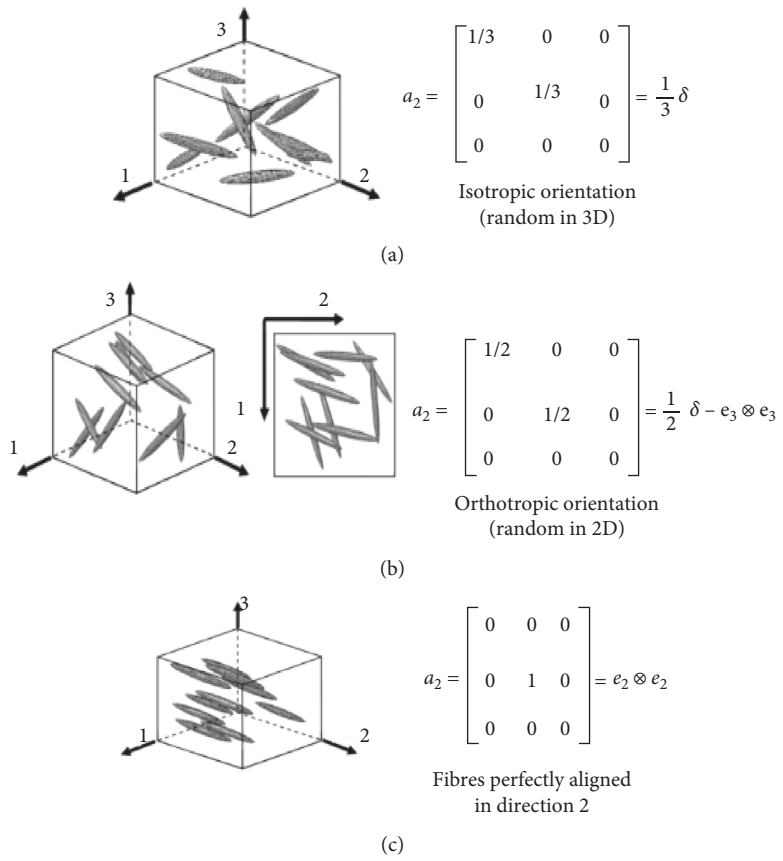

Figure 7: Examples of orientation: (a) random orientation in 3D, (b) random orientation in 2D, and (c) aligned orientation [32].

Table 6: Volume fraction and shape ratio for the four sizes of RVE.

RVE size (mm^3)	$40 \times 40 \times 40$	$50 \times 50 \times 50$	$60 \times 60 \times 60$	$70 \times 70 \times 70$
Shape ratio	2.405	2.75	2.59	2.37
Volume fraction	30.44	31.25	29.4	28.02

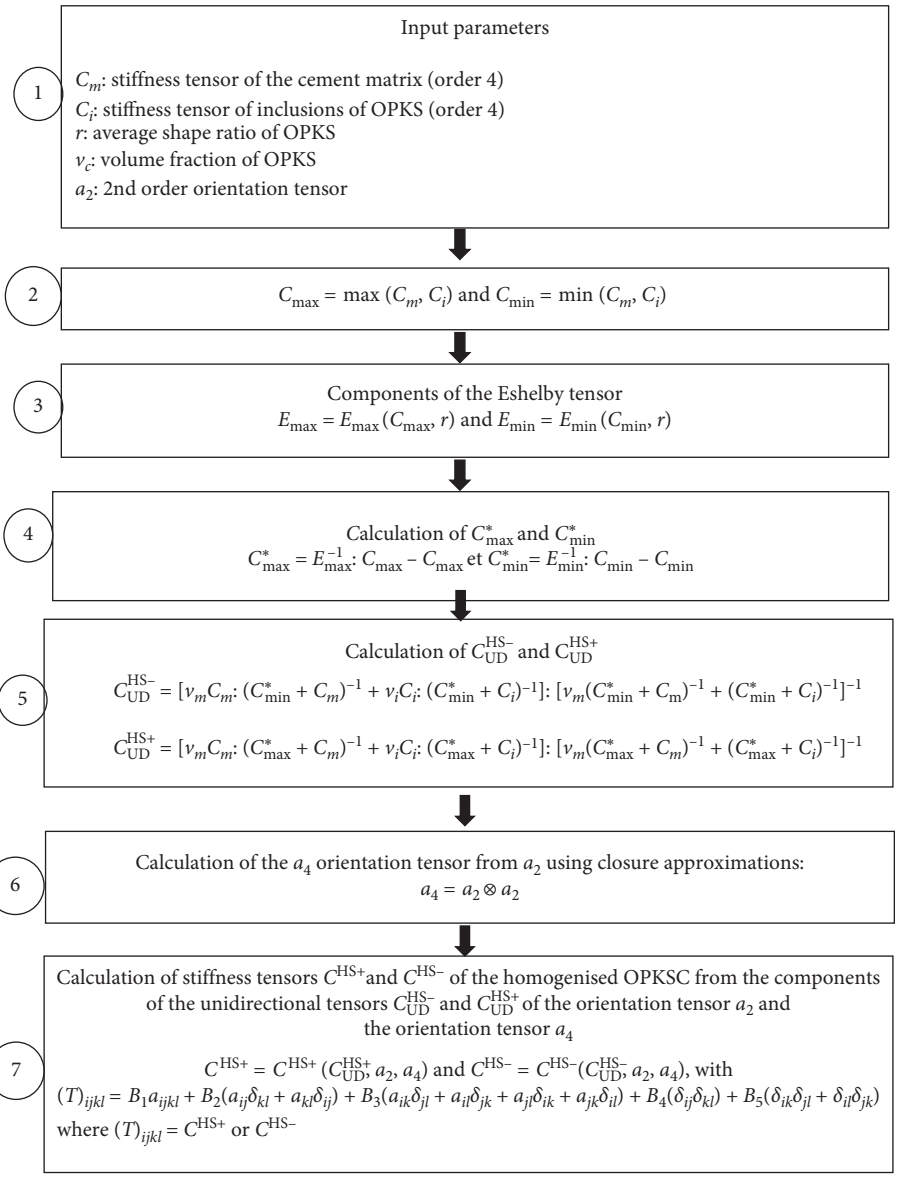

Figure 8: Determination of homogenised stiffness tensor (HS bounds).

We found that the volume fractions are nearly identical for the four experimentally designed RVE size types with a standard deviation of 1.21%. Thus, the results of Wiacek et al. [28] with respect to the size of the RVE (which must be five times larger than that of the particles) were confirmed. With a $11 \times 22\ cm^2$ sample, it was experimentally more difficult to obtain 70 mm side RVEs because of the grinding and smoothing operations of the sample. Hence, for the rest of the homogenisation process, we selected a cubic RVE with dimensions of $60 \times 60 \times 60\ mm^3$.

2.2.3. Step 3: Homogenisation. This step involved determining the equivalent behaviour of the heterogeneous material. The effective properties of the material related the average stress field σ to the average deformation field ε, calculated in the RVE. The constitutive relation for the heterogeneous material is given by

$$\begin{cases} \sigma = C : \varepsilon, \\ \varepsilon = S : \sigma, \end{cases} \tag{6}$$

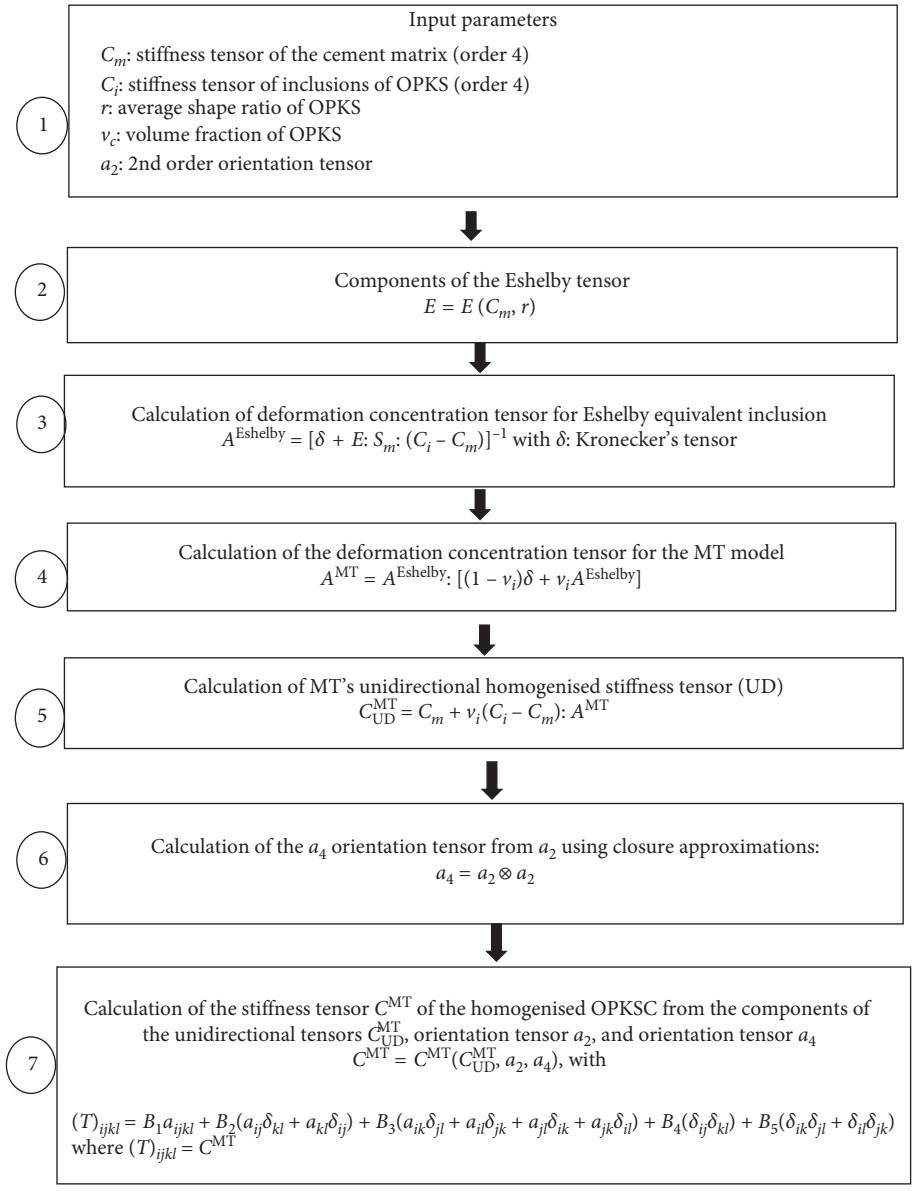

Figure 9: Determination of homogenised stiffness tensor (MT's approach).

where C is the tensor of the elastic stiffnesses (of order 4) and S is the tensor of elastic flexibilities (of order 4). Based on the assumptions that the composite was considered isotropic and elastic and by considering the boundary conditions of the RVE (homogeneity and compatibility), we obtained the equivalent stiffness tensor C of the composite, which is expressed as a function of the stiffness tensors of each phase and tensors of localisation A of the deformation in each phase [19]. This localisation tensor depends on homogenisation models, such as Voigt and Reuss, HS, MT, and the self-coherent model, which were constructed on the basis of the Eshelby inclusion problem [33, 34].

We have determined the stiffness tensors of the OPKS composite from the HS and MT models of resolution algorithms.

The diagrams of the MT and HS models are shown in Figures 8 and 9.

After the use of the homogenisation techniques, a stiffness tensor of order 4 was obtained. This stiffness tensor was transformed into a matrix form by means of the Voigt notation [35]. Thus, we obtained a definition in the form of equation (1), presented in Section 2.2. By comparing the components of the matrix resulting from the calculation based on Figures 4 and 5, and from the general expression of the stiffness matrix, Lame's coefficients were determined, from which the elastic properties of the OPKSC (Young's modulus and Poisson's ratio) were deduced.

The algorithms of HS and MT were transcribed in numerical calculation code executed by Mathematica 9 software (see Section 2 in Supplementary Materials). The calculation code developed in the present study was validated by comparing the results obtained by this code with those obtained by Nguyen using Nguyen's values as input values [19]. The results are presented in Table 7.

Table 7: Validation of Mathematica calculation code for homogenisation.

MT's model			HS's model (lower bound)			HS's model (upper bound)		
Values obtained by the calculation code	Values obtained by Nguyen	Difference	Values obtained by the calculation code	Values obtained by Nguyen	Difference	Values obtained by the calculation code	Values obtained by Nguyen	Difference
17.432	17.436	−0.02%	17.432	17.436	−0.02%	45.878	45.867	0.02%

Table 8: Young's modulus and Poisson's ratio, obtained from the approximations of HS and MT with $r = 2.591$ and $v_c = 29.40\%$ for the cubic RVE of $60 \times 60 \times 60\ mm^3$.

Phases	Young's modulus, E (GPa)	Poisson's ratio ν
OPKS	2.25 [24]	0.19 [25]
Cement paste	10.00 [26]	0.19 [26]
Composite OPKSC (HS)	6.34–6.96	0.17–0.17
Composite OPKSC (MT)	6.96	0.17

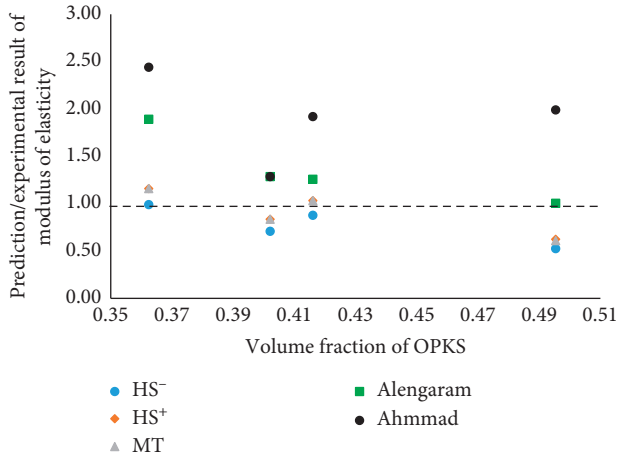

Figure 10: Variation in the ratio of the predicted to the experimental MoE values according to the volume fraction of OPKS.

3. Results and Discussions

3.1. Young's Modulus and Poisson's Ratio of OPKSC. Using the average values of the volume fractions and shape ratios of the OPKSs, obtained on the faces of the cubic RVE of $60 \times 60 \times 60\ mm^3$, Young's modulus and Poisson's ratio estimated by the approximations of HS and MT are summarised in Table 8.

Young's modulus, determined by MT's approximation (6.964 GPa), was very close to the upper bound determined by HS's approximation (6.956 GPa). This is in accordance with Benveniste's [36] interpretation of the MT model compared to the HS bounds predictions in the case of isotropic constituents and randomly oriented particles. He stated that when the matrix is in the most rigid phase, the MoE of the composite defined by the MT's method corresponds to the upper bound of the HS value, and when the matrix is in the most flexible phase, the MoE corresponds to the lower bound of the HS value. In this study, the cement matrix was in the most rigid phase of the composite. For Poisson's ratio, the value obtained by the MT approximation (0.167) for the OPKSC was sufficiently close to the values of Poisson's ratio (0.19) of the two phases of the said composite. The HS's approximation gave values close to Poisson's ratio (0.166–0.174) of the two constituent phases of the OPKSC, as obtained from the literature. The values of Young's modulus of the composite obtained by the two approximations were between those of the two phases with a remarkable proximity to that of the cement matrix. This was explained by the fact that it was the cement paste that was the dominant phase in the composition of the composite from the point of view of the stiffness and volume fraction.

To demonstrate the suitability of predicting the MoE of OPKSC by the homogenisation techniques (HS and MT), Figure 10 shows a comparison of the E-values of OPKSC with those predicted using the equations proposed by Alengaram [6] and Ahmmad [13], which are applicable for predicting values for concrete mixes with a compressive strength of up to 35 MPa and a density of up to $2000\ kg/m^3$. To make this comparison, we used certain experimental results reported in the literature, as shown in Table 9.

As can be seen in Figure 10, the ratios obtained using the values predicted by the homogenisation techniques (MT and HS) are closer to unity than those obtained by other prediction models for OPKSC with volume fractions of OPKS not exceeding 42%. Thus, the MoE of OPKSCs with various

Table 9: Experimental values for the physical and mechanical properties of OPKSC reported in the literature that are used for a comparison with the E-values estimated using homogenisation techniques.

Authors	Experimental data					
	Cementitious material content (kg/m^3)	Mix proportions C : S : OPKS	Specific density of OPKS (kg/m^3)	Density of hardened concrete (kg/m^3)	Cubic compressive strength (MPa)	Modulus of elasticity (GPa)
Teo et al. [11]	510	1 : 1.66 : 0.60	1170	1950	28.00	5.31
Alengaram et al. [6]	501	1 : 0.84 : 0.80	1270	1643	25.80	5.50
Alengaram et al. [6]	654	1 : 0.73 : 0.73	1270	1799	30.70	8.27
Mannan and Ganapathy [12, 37]	480	1 : 1.71 : 0.77	1170	1890	24.22	7.60

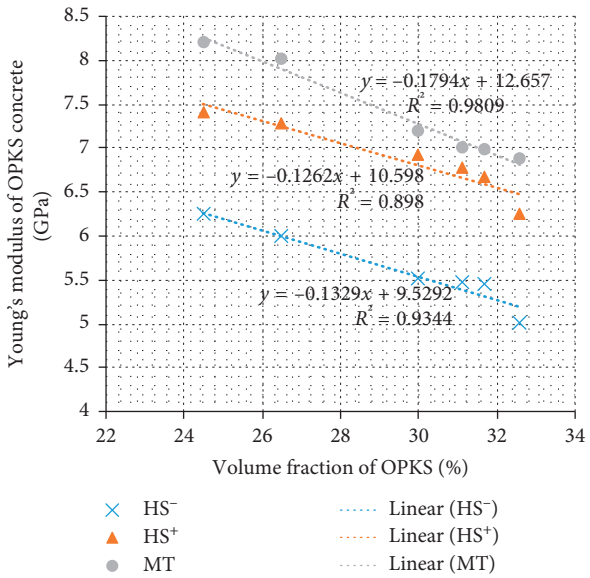

Figure 11: Variation in Young's modulus E as a function of volume fraction v_c of OPKS in concrete.

volume fractions estimated by the homogenisation techniques (MT and HS) in previous studies showed a good correlation with the experimental results. Therefore, it is also possible to use these homogenisation techniques (MT and HS) to estimate the mechanical properties of OPKSC; these techniques are advantageous in that they take into account the stiffnesses of the two phases of the composite, the volume fraction, the shape, and the orientation of the inclusions (OPKS).

3.2. Influence of the Volume Fraction of OPKS on Young's Modulus of OPKSC. In Figure 11 below, the values of the volume fraction considered were those obtained after the morphological study on the faces of the RVE, which ranged from 24.5% to 32.6%. Young's modulus variation curves for both homogenisation approaches had an almost linear form with $R^2 \geq 0.90$, which decreased as the volume fraction increased. The linearity of the decay of the curves was explained by the fact that the stiffness of the OPKS is lower than that of the cement matrix. Consequently, the more the OPKS is in the mix, the lower is the stiffness of OPKSC. An empirical linear correlation between the volume fraction of inclusions and the MoE was obtained from the mathematical expressions of the regression lines of the curves in Figure 11. This implies that if the results of a theoretical mixture proportioning of OPKSC are available, as in the approach proposed in [21], it is possible to estimate Young's modulus of the concrete; this enables the easy execution of the analysis of structural elements in lightly loaded buildings, based on OPKSC.

4. Conclusion

We estimated the elastic properties of OPKSC based on HS's and MT's micromechanical models. OPKSC is a composite material comprising two phases, namely, cement mortar matrix and inclusions of OPKS. The determination of its elastic properties by the homogenisation techniques required the knowledge of the elastic characteristics of each of these phases as well as other parameters, such as the volume fraction, average shape ratio, and orientation of the inclusions. The MoE of OPKSCs with various volume fractions ($f_{cu} < 35$ MPa and OPKS volume fraction < 42%) estimated by the homogenisation techniques (MT and HS) in previous studies showed a good correlation with the experimental results. These homogenisation approaches highlighted the influence of the increase in the volume of the composite particles on the stiffness. An empirical linear correlation was obtained between the volume fraction of the OPKS particles and Young's modulus of the composite. Hence, from the theoretical mixture proportioning of the composite, it is possible to predict the values of the elasticity constants of the OPKSC, which could facilitate the structural analysis of building elements in tropical countries producing palm oil.

Data Availability

The exhaustive data obtained from ImageJ analysis used to support the findings of this study are included in Supplementary Materials. The editable version of the numerical calculation code used to support the findings of this study is included in Supplementary Materials. The other experimental data used to support the findings of this study are included in the article.

Conflicts of Interest

The authors declare that they have no conflicts of interest.

Supplementary Materials

Section 1 deals with the exhaustive geometrical data obtained from the ImageJ analysis carried out on the face 1 of the RVE $60 \times 60 \times 60\,\text{mm}^3$. Section 2 presents the editable version of the numerical calculation code for the Hashin–Shtrikman's and Mori–Tanaka's algorithms for homogenisation of elastic properties of OPKSC. (*Supplementary Materials*)

References

[1] L. Yanjun, *Strength, Modulus of Elasticity, Shrinkage and Creep of Concrete*, University of Florida, Gainesville, FL, USA, 2007, http://ufdcimages.uflib.ufl.edu/UF/E0/02/15/79/00001/liu_y.pdf.

[2] A. Abdullah, "Basic strength properties of lightweight concrete using agricultural wastes as aggregates," in *Proc. Int. Conf. Low-Cost Hous. Dev. Ctries.*, Roorkee, India, 1984.

[3] D. C. Okpala, "Palm kernel shell as a lightweight aggregate in concrete," *Building and Environment*, vol. 25, no. 4, pp. 291–296, 1990.

[4] M. A. Mannan and C. Ganapathy, "Long-term strengths of concrete with oil palm shell as coarse aggregate," *Cement and Concrete Research*, vol. 31, no. 9, pp. 1319–1321, 2001.

[5] D. C. L. Teo, M. A. Mannan, and J. V. Kurian, "Flexural behaviour of reinforced lightweight concrete beams made with oil palm shell (OPS)," *Journal of Advanced Concrete Technology*, vol. 4, no. 3, pp. 459–468, 2006.

[6] U. J. Alengaram, H. Mahmud, and M. Z. Jumaat, "Enhancement and prediction of modulus of elasticity of palm kernel shell concrete," *Materials & Design*, vol. 32, no. 4, pp. 2143–2148, 2011.

[7] M. Gibigaye, G. F. Godonou, R. Katte, and G. Degan, "Structured mixture proportioning for oil palm kernel shell concrete," *Case Studies in Construction Materials*, vol. 6, pp. 219–224, 2017.

[8] P. Shafigh, M. Z. Jumaat, and H. Mahmud, "Mix design and mechanical properties of oil palm shell lightweight aggregate concrete : a review," *International Journal of Physical Sciences*, vol. 5, pp. 2127–2134, 2010.

[9] U. J. Alengaram, B. A. A. Muhit, M. Z. b. Jumaat, and M. Zamin, "Utilization of oil palm kernel shell as lightweight aggregate in concrete - a review," *Construction and Building Materials*, vol. 38, pp. 161–172, 2013.

[10] H. Mahmud, M. Z. Jumaat, and U. J. Alengaram, "Influence of sand/cement ratio on mechanical properties of palm kernel shell concrete," *Journal of Applied Sciences*, vol. 9, no. 9, pp. 1764–1769, 2009.

[11] D. C. L. Teo, M. A. Mannan, V. J. Kurian, and C. Ganapathy, "Lightweight concrete made from oil palm shell (OPS): structural bond and durability properties," *Building and Environment*, vol. 42, no. 7, pp. 2614–2621, 2007.

[12] M. A. Mannan and C. Ganapathy, "Engineering properties of concrete with oil palm shell as coarse aggregate," *Construction and Building Materials*, vol. 16, no. 1, pp. 29–34, 2002.

[13] R. Ahmmad, M. Z. Jumaat, S. Bahri, and A. B. M. S. Islam, "Ductility performance of lightweight concrete element containing massive palm shell clinker," *Construction and Building Materials*, vol. 63, pp. 234–241, 2014.

[14] J. K. Prusty and S. K. Patro, "Properties of fresh and hardened concrete using agro-waste as partial replacement of coarse aggregate—a review," *Construction and Building Materials*, vol. 82, pp. 101–113, 2015.

[15] P. Shafigh, H. B. Mahmud, M. Z. B. Jumaat, R. Ahmmad, and S. Bahri, "Structural lightweight aggregate concrete using two types of waste from the palm oil industry as aggregate," *Journal of Cleaner Production*, vol. 80, pp. 187–196, 2014.

[16] M. Aslam, P. Shafigh, M. Z. Jumaat, and M. Lachemi, "Benefits of using blended waste coarse lightweight aggregates in structural lightweight aggregate concrete," *Journal of Cleaner Production*, vol. 119, pp. 108–117, 2016.

[17] K. H. Mo, U. J. Alengaram, and M. Z. Jumaat, "Experimental investigation on the properties of lightweight concrete containing waste oil palm shell aggregate," *Procedia Engineering*, vol. 125, pp. 587–593, 2015.

[18] K. Hung, U. J. Alengaram, P. Visintin, S. Heng, and M. Zamin, "Influence of lightweight aggregate on the bond properties of concrete with various strength grades," *Construction and Building Materials*, vol. 84, pp. 377–386, 2015.

[19] H. G. Nguyen, S. Ortola, and E. Ghorbel, "Micromechanical modelling of the elastic behaviour of polymer mortars," *European Journal of Environmental and Civil Engineering*, vol. 17, no. 2, pp. 65–83, 2013.

[20] Y. Ke, S. Ortola, A. L. Beaucour, and H. Dumontet, "Identification of microstructural characteristics in lightweight aggregate concretes by micromechanical modelling including the interfacial transition zone (ITZ)," *Cement and Concrete Research*, vol. 40, no. 11, pp. 1590–1600, 2010.

[21] M. Gibigaye and G. F. Godonou, "Mixture proportioning for oil palm kernel shell," in *Oil Palm*, pp. 133–146, IntechOpen, London, UK, 2018.

[22] V. Preault, R. Corcolle, L. Daniel, and L. Pichon, "Effective permittivity of shielding composite materials for microwave frequencies," *IEEE Transactions on Electromagnetic Compatibility*, vol. 55, no. 6, pp. 1178–1186, 2013.

[23] M. Bornert, T. Bretheau, and P. Gilormini, *Homogénéisation en mécanique des matériaux, Tome 1 : Matériaux aléatoires élastiques et milieux périodiques*, Hermes sci, hal-00112720, 2001.

[24] S. Andrew, *CEB-FIP Manual of Lightweiqht Aggregate Concrete, Design and Technology*, Longman Group Ltd., London, UK, 1977.

[25] J. Müller-Rochholz, "Determination of the elastic properties of lightweight aggregate by ultrasonic pulse velocity measurement," *International Journal of Cement Composites and Lightweight Concrete*, vol. 1, no. 2, pp. 87–90, 1979.

[26] I. Yurtdas, "Couplage comportement mecanique et dessication des materiaux a matrice cimentaire: etude experimentale sur mortiers," thèse de Doctorat, Université des Sciences et Technologies de Lille (France), Villeneuve-d'Ascq, France, 2003, https://ori-nuxeo.univ-lille1.fr/nuxeo/site/esupversions/71967fc5-1bc9-4857-9c91-d072da81c958.

[27] I. Yurtdas, N. Burlion, and F. Skoczylas, "Triaxial mechanical behaviour of mortar: effects of drying," *Cement and Concrete Research*, vol. 34, no. 7, pp. 1131–1143, 2004.

[28] J. Wiacek, M. Molenda, J. Y. Ooi, and J. Favier, "Experimental and numerical determination of representative elementary volume for granular plant materials," *Granul. Matter*, vol. 14, pp. 449–456, 2012.

[29] S. Nemat-Nasser and M. Hori, *Applied Mathematics and Mechanics: Overall Properties Os Heterogeneous Materials*,

Elsevier Science Publishers B.V., Amsterdam, Netherlands, 1993.

[30] V. Picandet, P. Tronet, and C. Baley, "Caractérisation granulométrique des chènevottes," in *XXX e Rencontre l'Association Univ. Génie Civ.*, Chambéry (France), 2012, https://www.researchgate.net/publication/265728834_Caracterisation_granulometrique_des_chenevottes.

[31] W. H. Walton, "Feret's statistical diameter as a measure of particle size," *Nature*, vol. 162, no. 4113, pp. 329-330, 1948.

[32] S. G. Advani and C. L. Tucker, "The use of tensors to describe and predict fiber orientation in short fiber composites," *Journal of Rheology*, vol. 31, no. 8, pp. 751–784, 1987.

[33] J. D. Eshelby, "The determination of the elastic field of an ellipsoidal inclusion, and related problems," *Proceedings of the Royal Society of London. Series A. Mathematical and Physical Sciences*, vol. 241, pp. 376–396, 1957.

[34] J. D. Eshelby, "The elastic field outside an ellipsoidal inclusion," *Proceedings of the Royal Society of London. Series A. Mathematical and Physical Sciences*, vol. 252, no. 1271, pp. 561–569, 1959.

[35] R. M. Jones and R. Millard, *Mechanics of Composite Materials*, Library of Congress Cataloging-in-Publication Data, 2nd edition, 1999.

[36] Y. Benveniste, "A new approach to the application of Mori-Tanaka's theory in composite materials," *Mechanics of Materials*, vol. 6, no. 2, pp. 147–157, 1987.

[37] M. A. Mannan and C. Ganapathy, "Mix design for oil palm shell concrete," *Cement and Concrete Research*, vol. 31, no. 9, pp. 1323–1325, 2001.